Supplementary Information

Calculation of the absorbed fluence

To determine the absorbed fluence, we consider a sample thickness $t = 150$ nm and an absorption length of either $l_{780\,\mathrm{nm}} = 1.5$ μm and $l_{1200\,\mathrm{nm}} = 30$ μm. Since $t \ll l_{780\,\mathrm{nm}}$, $l_{1200\,\mathrm{nm}}$, the absorbed fluence fraction can be approximated as t/l_λ. Thus, 10 % and 0.5 % of the incident fluence are absorbed at 780 nm and 1200 nm, respectively.

Equilibrium spin Hamiltonian

The magnetic structure of Cu_2OSeO_3 consists at the microscopic level of 16 Cu ions per unit cell, each carrying a magnetic moment of $|\mathbf{s}_i| \approx \hbar/2$. However, due a hierarchy of magnetic interaction strengths [1], the four spins on each pyramid of the pyrochlore lattice bind together to form effective magnetic moments of size $|\mathbf{S}_i| = \hbar$ living on a trillium lattice. After an additional coarse graining step, valid for magnetic structures where the magnetization is constant over distances comparable with the lattice size ($\nabla \cdot \mathbf{M} \ll a$), the effective spin Hamiltonian in equilibrium is

$$H_0 = \sum_{\langle ij \rangle} \left[J\, \mathbf{m}_i \cdot \mathbf{m}_j + \mathbf{D}_{ij} \cdot (\mathbf{m}_i \times \mathbf{m}_j) \right] + \sum_i \mathbf{B} \cdot \mathbf{m}_i. \tag{1}$$

For Cu_2OSeO_3 the skyrmion radius is $r = 50.89$ nm, compared to the lattice parameter $a = 8.91$ Å, such that the coarse graining procedure is justified. To describe the magnetization dynamics we employ a three-dimensional square lattice with $40 \times 40 \times 10$ lattice points. The magnetic moments are normalized to $|\mathbf{m}_i| = 1$, and all interaction parameters are measured in units of the exchange interaction $J_0 = 48.2$ meV. This gives the effective parameters $J = 1$, $D = 0.224$ and $B = 0.013$, corresponding to 20.7 mT, in agreement with previous work [1].

Simulated annealing and Metropolis Monte Carlo

The equilibrium magnetic phase diagram is found by simulated annealing down to a target temperature $k_B T/J_0 = 0.02$ using the Metropolis Monte Carlo algorithm [2], corresponding to $T \approx 1$ K. To minimize stochastic effects in the phase diagram and the subsequent dynamics, each step involves 2000 thermalization sweeps followed by an average over 2000 Monte Carlo realizations with 40 sweeps each. In agreement with previous work [3], and as illustrated in Figure S1, we find four competing equilibrium phases: a ferromagnetic phase, a helical spiral phase, a conical phase and a skyrmion crystal (SkX) phase.

Equations of motion

The magnetization dynamics is governed by the Landau-Lifshitz-Gilbert (LLG) equation [4, 5], which in the present case reads

$$\frac{\partial \mathbf{m}_i}{\partial t} = -\gamma \mathbf{m}_i \times \frac{\delta H}{\delta \mathbf{m}_i} - \lambda \mathbf{m}_i \times \left(\mathbf{m}_i \times \frac{\delta H}{\delta \mathbf{m}_i} \right). \tag{2}$$

Here the effective magnetic field acting on magnetic moment $\mathbf{m}_i$ is given by the functional derivative of the total Hamiltonian H with respect to $\mathbf{m}_i$. The parameters $\gamma = 1/(1+\alpha^2)$ and $\lambda = \alpha/(1+\alpha^2)$ take into account the phenomenological damping constant α, which for Cu_2OSeO_3 is on the order of 10^{-4}. The LLG equation is solved by geometric Depondt-Mertens algorithm [6].

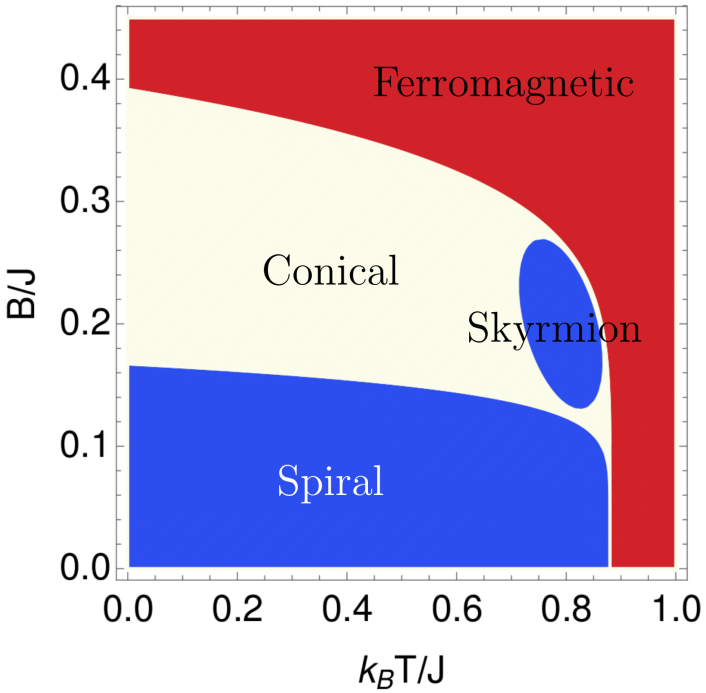

Figure S1: **Magnetic phase diagram of Cu_2OSeO_3.** Schematic magnetic phase diagram for $J = 1$ and $D = 0.224$ as a function of thermal energy k_BT and magnetic field B. The phase boundaries were obtained by simulated annealing with the Metropolis Monte Carlo method.

Light-matter coupling

The dominant light-matter coupling mechanisms considered here are Raman excitation of phonons and magnons, an effective magnetic field generated by the inverse Faraday effect, and a direct magneto-electric coupling via the spontaneous polarization [7–9]. Several studies have found a strong dependence of the Dzyaloshinskii-Moriya interaction (DMI) on strain [10, 11] as well as on a dynamical coupling to acoustic phonons [12]. To describe such mechanisms we consider the total Hamiltonian $H(t) = H_0 + H_I(t)$, with the time-dependent interaction Hamiltonian

$$H_I(t) = \sum_{\langle ij \rangle} \left[J_{ij}(t) \mathbf{m}_i \cdot \mathbf{m}_j + \mathbf{D}_{ij}(t) \cdot (\mathbf{m}_i \times \mathbf{m}_j) \right] + \sum_i \left[\mathbf{B}(t) \cdot \mathbf{m}_i - \mathbf{E}(t) \cdot \mathbf{P}_i \right], \tag{3}$$

The exchange interaction $J_{ij} = g_{\mathrm{R}}(t)(\mathbf{e}_{\mathrm{sc}} \cdot \mathbf{d}_{ij})(\mathbf{e}_{\mathrm{in}} \cdot \mathbf{d}_{ij})$ is modified to take into account magnon Raman processes, the inverse Faraday effect generates an effective field $\mathbf{B}(t) = g_{\mathrm{IFE}} \mathbf{E}^*(t) \times \mathbf{E}(t)$, and the magneto-electric effect is described by a coupling to the polarization $\mathbf{P}_i = g_{\mathrm{m-el}}(S_i^y S_i^z, S_i^z S_i^x, S_i^x S_i^y)$. Assuming a uniform excitation of acoustic phonons with momenta $\mathbf{k} \approx 0$ gives an isotropic modification of the DMI strength $\mathbf{D}(t) = \mathbf{D}(1 - g_{\mathrm{m-ph}}(t))$, where $g_{\mathrm{m-ph}}(t)$ is proportional to the time-dependent average phonon amplitude. Since the phonon dynamics of Cu_3OSeO_2 is very complex, we here use a phenomenological description of $g_{\mathrm{m-ph}}(t)$ as a log-normal function, with an onset determined by the laser electric field and a decay related to the phonon lifetime τ_{ph}. The laser electric field is described by a normalized Gaussian envelope of width σ and peak time τ.

Time-dependence of the magnetic parameters

The excitation mechanisms discussed above are associated with different characteristic time-scales. In particular, both the magnon Raman processes, inverse Faraday effect and magneto-electric effects are impulsive in the sense that they only are present during the action of the laser pulse. In contrast, the magnon-phonon coupling is expected to persist for as long as there are phonons in the system. Since

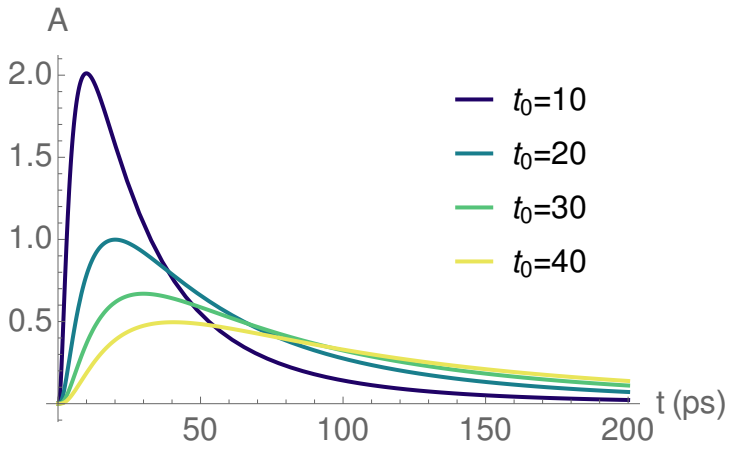

Figure S2: **Time-dependence of magnon-phonon interaction.** Examples of log-normal functions with peak time t_0 as used to model time-dependence of the magnon-phonon interaction.

the magnetic moments have a characteristic time-scale of about 1 ps, while a single optical cycle of the laser is around 1 fs, the magnetic moments are assumed to only respond to the average field given by the pulse envelope.
Under these assumptions, the first three mechanisms satisfy $g_i(t) = g_i f(t)$ for $g_i \in \{g_{\mathrm{R}}, g_{\mathrm{IFE}}, g_{\mathrm{m-el}}\}$ and can be described by a Gaussian time-dependence of the form

$$f(t) = \frac{1}{\tau\sqrt{2\pi}} \exp[-(t-t_0)^2/(2\tau^2)], \tag{4}$$

where τ is the pulse width and t_0 the time of peak intensity. In contrast, the magnon-phonon coupling is modeled by the log-normal function

$$g_{\mathrm{m-ph}}(t) = \frac{g_{\mathrm{m-ph}}}{t\sigma\sqrt{2\pi}} \exp[-(\ln t - \mu)^2/(2\sigma^2)] \tag{5}$$

Here the peak time is given by $t_0 = e^{\mu-\sigma^2}$, and the effective width (or skewness) by $\tau = (e^{\sigma^2}+2)\sqrt{e^{\sigma^2}-1}$. The width is assumed to be related to the phonon lifetime, which is assumed to be of the order of 100 ps. A few examples of the log-normal function for $\sigma = 1$ and different t_0 is given in Figure S2.

Definition of the topological charge

To quantify the topology of the spin texture we use the lattice topological charge Q defined by [13]

$$Q = \frac{1}{4\pi} \sum_{\Delta} \Omega_{\Delta}. \tag{6}$$

In this definition the lattice is triangulated and Ω_Δ corresponds to the signed area of the spherical triangle spanned by three neighboring spins, given by [13]

$$\exp(i\Omega_\Delta/2) = \frac{1}{\rho}(1 + \mathbf{m}_i\cdot\mathbf{m}_j + \mathbf{m}_j\cdot\mathbf{m}_k + \mathbf{m}_k\cdot\mathbf{m}_i + i\eta_{ijk}\mathbf{m}_i\cdot[\mathbf{m}_j\times\mathbf{m}_k]) \tag{7}$$
$$\rho = \sqrt{2(1+\mathbf{m}_i\cdot\mathbf{m}_j)(1+\mathbf{m}_j\cdot\mathbf{m}_k)(1+\mathbf{m}_k\cdot\mathbf{m}_i)},$$

where $\eta_{ijk} = +1$ (-1) if the path $i \to j \to k \to i$ is positively (negatively) oriented. The surface area Ω_Δ is well-defined everywhere except at the zero-measure set $\mathbf{m}_i\cdot(\mathbf{m}_j\times\mathbf{m}_k) = 0$ and $1+\mathbf{m}_i\cdot\mathbf{m}_j+\mathbf{m}_j\cdot\mathbf{m}_k+\mathbf{m}_k\cdot\mathbf{m}_i < 0$, where $\exp(i\Omega_\Delta/2)$ has a branch cut.
The topological charge is a compact, convenient indicator of the presence of a non-trivial spin texture: For a single skyrmion $Q = -1$, for a single antiskyrmion $Q = 1$, and for a cluster of skyrmions and antiskyrmions $Q = \sum_i Q_i$ with Q_i their individual charges.

Supplemental Note: Estimated magnitude of light-matter couplings

As discussed in detail in the following sections, the magnon Raman coupling gives a modulation $\sim$ 10 % of the equilibrium exchange, the inverse Faraday effect is likely negligible, the magneto-electric effect gives a contribution of around $\sim$ 1 % of the equilibrium exchange, while the spin-phonon coupling can give a modulation on the order of $\sim$ 50 % of the equilibrium DMI.

Magnon Raman processes

An isotropic light-matter interaction arises due to the coupling of the laser to the charge of the electrons underlying the magnetic moments. For spin-1/2 systems, this coupling can be derived by considering a half-filled Mott insulator subject to an external electric field. The weak-field limit of this coupling reproduces the Raman vertex derived by Fleury and Loudon from general symmetry arguments [14–16], and is described by the Raman Hamiltonian [17]

$$\begin{aligned} H_R &= \sum_{qq'} R_{\mathbf{q}\mathbf{q}'} a^\dagger_{q'} a_q \sum_{\langle ij \rangle} g_{ijqq'} \mathbf{m}_i \cdot \mathbf{m}_j \\ &= \sum_{\langle ij \rangle} J_{ij} \mathbf{m}_i \cdot \mathbf{m}_j. \end{aligned} \tag{8}$$

Here $R_{\mathbf{q}\mathbf{q}'} = J(ea/\hbar)^2 \gamma_{\mathbf{q}} \gamma_{\mathbf{q}'}$ is the strength of the Raman coupling, e is the electron charge, a the lattice parameter, $\hbar$ Planck's constant, and J is the equilibrium exchange interaction. The function $\gamma_{\mathbf{q}}$ describes the strength of the one-photon vector potential, and the geometric factor $g_{ijqq'} = (\hat{\mathbf{e}}^*_q \cdot \mathbf{d}_{ij})(\hat{\mathbf{e}}_{q'} \cdot \mathbf{d}_{ij})$ encodes the underlying virtual electronic processes. To simplify the notation we have defined $q \equiv \{\mathbf{q}, s\}$ with s the polarization.
The leading order term of the Raman Hamiltonian describes a two-photon two-magnon process. To assess the strength of the light-matter coupling, we note that $\lambda_{R,\mathbf{q}} = R_{\mathbf{q}\mathbf{q}'} n_{\mathbf{q}}$ where $n_{\mathbf{q}}$ is the number of photons in the incident field. Using the fact that $n_{\mathbf{q}} = IV/(\hbar\omega_{\mathbf{q}} c)$ with the intensity $I = (cn\epsilon_0/2)E^2$, we have $\lambda_{R,\mathbf{q}} = (ea/\hbar\omega_{\mathbf{q}})^2 (n/4) E^2$. Assuming that $a = 5$ Å, $E = 10^9$ Vm^{-1} and $n = 2.40$, we find $\lambda_R = 0.16$ with and characteristic energy scale $g_{\mathrm{R}} = J\lambda_R = 7.7$ meV.

Inverse Faraday effect

For a system with non-zero magnetization the dielectric tensor acquires nonzero off-diagonal elements and can be written as $\epsilon_{ij}(\mathbf{M}) = \epsilon_0(\epsilon_r \delta_{ij} - if\epsilon_{ijk} M_k)$. Here ϵ_0 is the vacuum permittivity, ϵ_r the relative permittivity, f is a small parameter related to the Faraday angle θ_F discussed below, and δ_{ij} and ϵ_{ijk} are the Kronecker and Levi-Cevita tensors, respectively. Calculating the interaction energy in a volume V_c around each spin [18–20],

$$U(t) = -\frac{i\theta_F c\sqrt{\epsilon_r}\epsilon_0 a^3}{2\omega} \frac{\mathbf{M}(\mathbf{r})}{M_s} \cdot [\mathbf{E}^*(t) \times \mathbf{E}(t)], \tag{9}$$

the Faraday coupling is $\alpha_F = \theta_F V_c c\sqrt{\epsilon_r}$, where θ_F is the Faraday angle per unit distance, and $\mathbf{B}_F(t) = \epsilon_0/(2i\omega)[\mathbf{E}^*(t) \times \mathbf{E}(t)]$ is the effective optical spin density. The IFE coupling Hamiltonian is then written as

$$H_{\mathrm{IFE}} = \alpha_F \mathbf{B}_F(t) \cdot \sum_i \mathbf{m}_i. \tag{10}$$

To estimate the light-matter coupling strength, we write the Faraday angle as $\theta_F = \mathcal{V}B$ where $\mathcal{V}$ is the so-called Verdet constant, which is smaller than 100 rad/Tm. Taking $E = 10^9$ V/m, $a = 5$ Å and $\lambda = 1240$ nm, giving $\hbar\omega = 1$ eV, we find the characteristic energy scale $g_{\mathrm{IFE}} = \alpha_F |\mathbf{B}_F| = 4.3 \times 10^{-4}$ meV.

Magnetoelectric coupling

Due to the multiferroic nature of Cu_2OSeO_3 there is a direct magnetoelectric coupling proceeding with $d-p$-hybridization [8]. The resulting magnetoelectric coupling Hamiltonian is

$$H_{\mathrm{m-el}} = -\mathbf{E}\cdot\sum_i \mathbf{P}_i \tag{11}$$
$$\mathbf{P}_i = \gamma(S_i^y S_i^z, S_i^z S_i^x, S_i^x S_i^y).$$

In Refs. [8, 9] the coupling constant γ is estimated to the value $\gamma = 5.64\cdot 10^{-27}$ μCm by comparison to experiment. This gives, for an electric field of $E = 10^9$ Vm^{-1}, an interaction energy of $g_{\mathrm{m-el}} \approx 10^{-23}$ J or equivalently $g_{\mathrm{m-el}} \approx 1$ meV.

Magnon-phonon coupling

The spin-phonon coupling of Cu_2OSeO_3 has been discussed in the context of non-reciprocal magnon propagation [12], where a coupling Hamiltonian of the form

$$H_{\mathrm{s-ph}} = \gamma D\partial_z u_x(S_i^y S_j^z - S_i^z S_j^y) + \gamma D\partial_z u_y(S_i^z S_j^x - S_i^x S_j^z) \tag{12}$$

was derived for a phonon propagating along the z-direction. Assuming acoustic phonons propagating along all cubic axes are excited with the same probability, this gives a spin-phonon coupling Hamiltonian

$$H_{\mathrm{s-ph}} = \gamma\mathbf{D}\cdot(\mathbf{S}_i\times\mathbf{S}_j) \tag{13}$$

where the DMI vector has been shifted according to the following

$$\begin{aligned} D_x &= D_{x0}(1+\gamma[\partial_y+\partial_z]u_x) \\ D_y &= D_{y0}(1+\gamma[\partial_z+\partial_x]u_y) \\ D_z &= D_{z0}(1+\gamma[\partial_x+\partial_y]u_z). \end{aligned} \tag{14}$$

To estimate the size of the DMI modulation, we note that in Ref. [12] the value of γ was estimated to be in the range $\gamma = 50-90$ by fitting the calculated magneto-chiral effect towards experiment. With an estimate of the phonon derivatives of $\partial_j u_i \approx k_j u_i \approx 0.01$, the spin-phonon coupling can still give a modulation of the DMI on the order of 50 %. This gives a characteristic energy scale of $g_{\mathrm{m-ph}} = 0.5D = 5.4$ meV. This large value is in line with previous studies, where the strain-induced modulation of the DMI has been found to be very large for a number of chiral magnets [10, 11].
Although the time-dependence of the phonon coordinate u could in principle be obtained by a full dynamical simulation of the coupled vibrational modes of Cu_2OSeO_3, such a calculation becomes prohibitive in practice due to the complexity of the system. Here we instead take a phenomenological approach and parameterize the time-dependence of the DMI with a log-normal function, whose onset is determined by the pulse parameters of the laser electric field and whose decay is set by the lifetime of the phonon modes.

References

[1] O. Janson, I. Rousochatzakis, A. A. Tsirlin, M. Belesi, A. A. Leonov, U. K. Rößler, J. van den Brink, H. Rosner, *Nature Communications* **2014**, *5*, 1.

[2] E. V. Boström, C. Verdozzi, *Phys. Status Solidi B* **2019**, *256*, 7 1800590.

[3] S. Buhrandt, L. Fritz, *Phys. Rev. B* **2013**, *88* 195137.

[4] M. Lakshmanan, *Philos. Trans. Royal Soc. A* **2011**, *369*, 1939 1280.

[5] V. G. Baryakhtar, B. A. Ivanov, *Low Temp. Phys.* **2015**, *41*, 9 663.

[6] P. Depondt, F. G. Mertens, *Journal of Physics: Condensed Matter* **2009**, *21*, 33 336005.

[7] J. H. Yang, Z. L. Li, X. Z. Lu, M.-H. Whangbo, S.-H. Wei, X. G. Gong, H. J. Xiang, *Phys. Rev. Lett.* **2012**, *109* 107203.

[8] S. Seki, X. Z. Yu, S. Ishiwata, Y. Tokura, *Science* **2012**, *336*, 6078 198.

[9] Y.-H. Liu, Y.-Q. Li, J. H. Han, *Phys. Rev. B* **2013**, *87* 100402.

[10] K. Shibata, J. Iwasaki, N. Kanazawa, S. Aizawa, T. Tanigaki, M. Shirai, T. Nakajima, M. Kubota, M. Kawasaki, H. S. Park, D. Shindo, N. Nagaosa, Y. Tokura, *Nature Nanotechnology* **2015**, *10*, 7 589.

[11] L. Deng, H.-C. Wu, A. P. Litvinchuk, N. F. Q. Yuan, J.-J. Lee, R. Dahal, H. Berger, H.-D. Yang, C.-W. Chu, *Proceedings of the National Academy of Sciences* **2020**, *117*, 16 8783.

[12] T. Nomura, X.-X. Zhang, S. Zherlitsyn, J. Wosnitza, Y. Tokura, N. Nagaosa, S. Seki, *Phys. Rev. Lett.* **2019**, *122* 145901.

[13] B. Berg, M. Lüscher, *Nucl. Phys. B* **1981**, *190*, 2 412 .

[14] B. S. Shastry, B. I. Shraiman, *Phys. Rev. Lett.* **1990**, *65* 1068.

[15] P. A. Fleury, S. P. S. Porto, R. Loudon, *Phys. Rev. Lett.* **1967**, *18* 658.

[16] P. A. Fleury, R. Loudon, *Phys. Rev.* **1968**, *166* 514.

[17] E. V. n. Boström, T. S. Parvini, J. W. McIver, A. Rubio, S. V. Kusminskiy, M. A. Sentef, *Phys. Rev. B* **2021**, *104* L100404.

[18] N. Ogawa, S. Seki, Y. Tokura, *Sci. Rep.* **2015**, *5*, 1 9552.

[19] R. Khoshlahni, A. Qaiumzadeh, A. Bergman, A. Brataas, *Phys. Rev. B* **2019**, *99* 054423.

[20] S. V. Kusminskiy, *Quantum Magnetism, Spin Waves, and Optical Cavities*, Springer International Publishing, **2019**.